AN IMPROVED DIFFRACTION TOMOGRAPHY FOR IMAGING OF HIGH-CONTRAST DIELECTRIC OBJECTS

Kyoung-Whoan Suh*, Se-Yun Kim**, and Jung-Woong Ra***

* SAMSUNG Electronics, Seoul, Korea
** Korea Institute of Science and Technology, Seoul, Korea
*** Korea Advanced Institute of Science and Technology, Daejeon, Korea

ABSTRACT

An improved version of diffraction tomography has been developed for microwave imaging of high-contrast dielectric objects. It consists of three steps. First the spatially sliced projection functions are constructed from frequency-diversity measurement data at a fixed angle. Then the domain of those projection functions is adjusted to the same area of the actual object. After angular-diversity measurements, high-contrast dielectric profiles are reconstructed by backprojecting the modified projection functions. Some numerical simulations are performed and those results are presented here.

INTRODUCTION

Soon after Lasen and Jacobi (1) performed the experiments on active microwave imaging of a canine kidney in 1979, the realization of a microwave imaging system for medical diagnosis on human bodies has been tried by adopting diffraction tomography as a leading reconstruction algorithm. The physical mechanism on diffraction tomography has been well established by investigators (2-3). With plane wave illuminations of multi-frequencies in far-field region and the assumption of weak scattering objects under the Born approximation, the plane wave spectrum of the scattered fields consists of a circular arc in the Fourier transformed domain of the dielectric distribution over the object. The spectral space can be filled by performing the angular-diversity measurement. Hence, the reconstruction of object profiles consists of interpolation and the inverse FFT. The interpolation process, however, is considered as a key factor of the degradation in the retrieved image and of the consumption in computation time. In particular, the adoption of the Born or Rytov approximation in the derivation of the diffraction tomography becomes a key degrading factor on reconstruction of high-contrast biological bodies (4).

To overcome the above limitations posed in conventional diffraction tomography, we suggested an alternative algorithm compatible to microwave imaging of high-contrast dielectric objects (5). It can be derived by introducing the projection functions, which are constructed by integrating the permittivity distribution along the direction perpendicular to the range axis. For example, $p(\theta, u)$ in Fig. 1 is the projection function for mono-static case. Then, the projection function at a fixed direction can be obtained from frequency-diversity measurement. Repeating the measurement for different directions of illuminations, one may obtain all the projection functions which look like those in X-ray CT. Hence, the reconstruction of object profiles can be implemented by applying conventional CT algorithm to the projection functions. While the projection functions in X-ray CT are taken by integration of X-ray absorption along the direction of X-ray propagation, those in the presented algorithm are obtained from line integral along the normal direction to microwave propagation.

For a high-contrast dielectric object, the domain of its projection functions exceeds the physical bound of the object due to the limitation inherent to the first-order Born approximation. Hence, after reducing its maximum domain equal to the actual dimension of the object, one may obtain an improved profile by backprojecting the modified projection functions. Some numerical examples are presented here.

THEORY

Consider an inhomogeneous dielectric cylinder with relative dielectric constant ε_r

CH3277-1/93/0000-1141$01.00 © 1993 IEEE

(x,y) distributed over arbitrary cross-section S, as shown in Fig. 1. When an E-polarized wave u^i radiated from a mono-static antenna is incident on the cylinder toward positive u-axis, the scattered electric field u^s (x,y) may be written

$$u^s(x,y) = -\frac{jk^2}{4}\iint_S dx'dy' \,[\epsilon(x',y') - 1]\, u^t(x',y') \times H_0^{(2)}(k\sqrt{(x-x')^2 + (y-y')^2}), \quad (1)$$

where k is the free-space wavenumber, $H_0^{(2)}$ denotes the zeroth-order Hankel function of the second kind, and u^t means the total field. For convenience, the (x,y) coordinates are fixed at the cylinder, which is rotated by an angle θ with respect to the (u,v) coordinates. The variables u and v are the range and cross-range axes of the antenna, respectively.

If the mono-static T/R antenna is located far away from the cylinder, one may assume that u^i is equal to e^{-jku}. It implies that the equi-phase line of the incident field over S is parallel with the v-axis. Applying the first-order Born approximation to equation 1 yields a normalized backscattered field $\Gamma(\theta;\alpha)$ as

$$\Gamma(\theta;\alpha) = u^s(\rho_0) \times \sqrt{\frac{8\pi\rho_0}{k^3}}\, e^{j(k\rho_0 + \pi/4)} = \iint_{-\infty}^{\infty} du dv \,[\epsilon_r(u,v) - 1]\, e^{-j\alpha u}, \quad (2)$$

where ρ_0 is the distance between the antenna and the origin of the (x,y) coordinates and $\alpha = 2k$ is the function of the frequency. It should be noted that the integration range in equation 2 is extended to infinitely because $\epsilon_r(x,y)$ is 1.0 outside the cylinder.

Now, the projection function $p(\theta,u)$ is defined as

$$p(\theta;u) = \int_{-\infty}^{\infty} dv \,[\,\epsilon_r(u,v) - 1\,]. \quad (3)$$

Substitution of equation 3 into equation 2 yields

$$\Gamma(\theta;\alpha) = \int_{-\infty}^{\infty} du\; p(\theta;u)\, e^{-j\alpha u}. \quad (4)$$

Since equation 4 represents the relation of one-dimensional Fourier transform between $\Gamma(\theta;\alpha)$ and $p(\theta;u)$, the projection function $p(\theta;u)$ can be readily obtained from the normalized backscattered field as

$$p(\theta;u) = \frac{1}{2\pi}\int_{-\infty}^{\infty} d\alpha\, \Gamma(\theta;\alpha)\, e^{j\alpha u}. \quad (5)$$

In general, the necessary condition on the first-order Born approximation for mono-static measurement as shown in Fig. 1 is specified as

$$\Delta\sqrt{\epsilon_r} \times a < \frac{c}{8f}, \quad (6)$$

where a denotes the maximum dimension of dielectric cylinder and c is the velocity of the light in vacuum. The left term of equation 6 means that the high-contrast dielectric cylinder with the maximum dimension of a looks like a larger dielectric cylinder with low-contrast enough to satisfy the first-order Born approximation. Hence, if a high-contrast dielectric object as human bodies are under the microwave imaging by using the above algorithm, the u-domain of $p(\theta;u)$ may exceeds the actual boundary of S. To improve the quality of the projection functions, we adjust the maximum domain of $p(\theta;u)$ equal to the actual dimension of u inside S.

The remaining problem is how to reconstruct ϵ_r (x,y) from the projection function $p(\theta;u)$. As shown in equation 2, $p(\theta;u)$ is considered a tomographic projection of $(\epsilon_r - 1)$ distribution to the u-axis. The projection functions in the full angle of θ from 0° to 360° are calculated by performing angular-diversity measurements and taking the inverse Fourier transform in equation 5. Applying conventional CT algorithms to equation 4, one may obtain an image of ϵ_r (u,v). It should be mentioned that the convolution backprojection (6) with Shepp and Logan filter (7) is adopted here as CT algorithm.

SIMULATION RESULTS

As a typical example, the backscattered fields from a homogeneous dielectric cylinder of radius a = 10cm are calculated in the frequency range from f = 0.1 to 4.0 GHz with a fixed step of 0.1 GHz. Then, one may obtain normalized projection functions for the relative dielectric constant ϵ_r = 1.01, 1.1, 1.5, 2.0, 3.0, and 4.0, as shown in Fig. 2. One of interesting features in Fig. 2 is that the extents of projection functions keep the same size of the actual cylinder for ϵ_r = 1.01 and 1.1, but go out of its boundary as ϵ_r exceeds 1.5. The overflow of projection functions results from the limitation inherent to the first-order Born approximation. For Fig. 2 case, the Born approximation is valid under the restriction of the maximum value of ϵ_r less than about 1.2. If ϵ_r becomes larger than about 1.2, the presented diffraction tomography considers the frequency-diversity fields backscattered from the

larger cylinder of ε_r = 1.2, which is equivalent to the actual dielectric cylinder.

Performing the angular-diversity measurement, and the applying the convolution-backprojection to the projection functions, one may obtain the image of the dielectric cylinder, Figs. 3(a) and (b) show the images of a homogeneous dielectric cylinder with a = 10cm, ε_r = 1.1 and 2.0, respectively. As expected, the reconstructed image for ε_r = 2.0 is blurred. Such a degradation of images for high-contrast dielectric objects is the most critical drawback of active microwave imaging scheme based on the diffraction tomography.

In real situation on active microwave biological imaging, the actual boundary of a biological object is known previously. This pre-information helps the enhancement of the degraded image for ε_r larger than 1.2. As shown in Fig. 4, the fine image of the dielectric cylinder with a = 10cm and ε_r = 2.0 can be obtained by additionally reducing the overflowed extents of projection functions equal to the actual size of the dielectric cylinder.

CONCLUSIONS

An alternative algorithm of conventional diffraction tomography has been suggested for microwave imaging of high-contrast dielectric objects. The projection functions are introduced by integrating the permittivity distribution along the direction perpendicular to the range axis of mono-static antenna. Under the first-order Born approximation, a high-contrast dielectric object is considered as a low-contrast dielectric object with larger size. It leads us to adjust the domain of the projection functions for high-contrast dielectric objects equal to those actual size. Numerical simulations assure the validity of the presented diffraction tomography. In conclusion, the improved diffraction tomography may provide a stepstone to develop a microwave imaging system adapted to biological bodies by removing the limitation of the first-order Born approximation.

REFERENCES

(1) L. E. Larsen and J. H. Jacobi, "Microwave scattering parameter imagery of an isolated canine kidney, " Med. Phys., vol. 6, pp. 394-403, 1979.

(2) E. Wolf, " Three-dimensional structure determination of semi-transparent objects from holographic data, " Opt. Communicat., vol. 1, pp. 153-156, 1969.

(3) A. J. Devaney, " A filtered backpropagation algorithm for diffraction tomography, " Ultrasonic Imagimg, vol. 4, pp. 336-350, 1982.

(4) M. Slaney, A. C. Kak, and L. E. Larsen, " Limitations of imaging with first-order diffraction tomography, " IEEE Trans. Microwave Theory Tech., vol. MTT-32, pp. 860-874, 1984.

(5) K. W. Suh, S. Y. Kim, and J. W. Ra, " A new spatial slice theorem for microwave imaging, " Microwave Optical Tech. Lett., vol. 3, pp. 362-365, 1990.

(6) R. M. Mersereau and A. V. Oppenheim, " Digital reconstruction of multidimensional signals from their projections, " Proc. IEEE, vol. 62, pp. 1319-1338, 1978.

(7) L. A. Shepp and B. F. Logan, " The Fourier reconstruction of a head section, " IEEE Trans. Nucl. Sci., vol. NS-21, pp. 21-43, 1974.

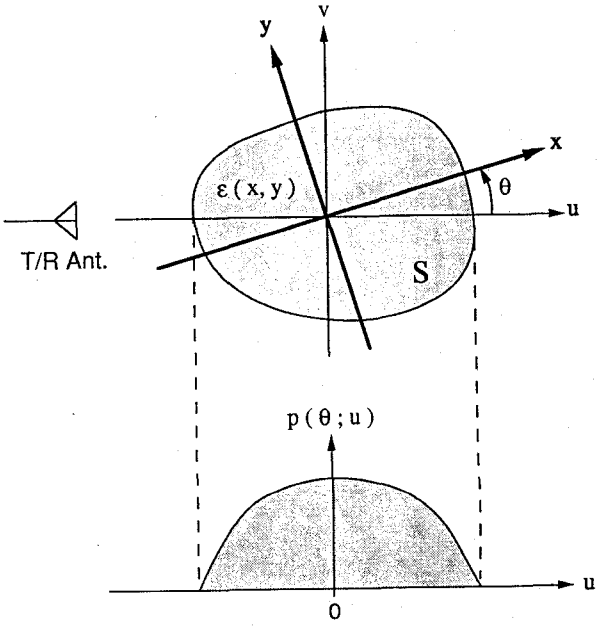

Fig. 1 The object geometry and its projection for microwave imaging.

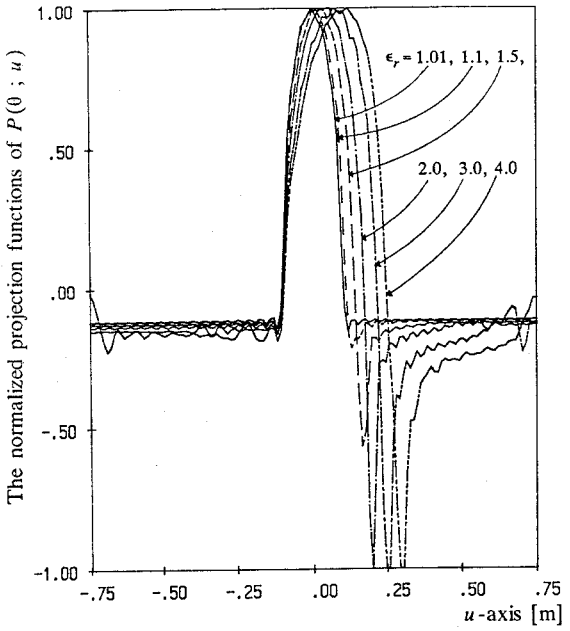

Fig. 2 The normalized projection functions for a homogeneous dielectric cylinder of radius 10cm and ε_r =1.01, 1.1, 1.5, 2.0, 3.0, and 4.0.

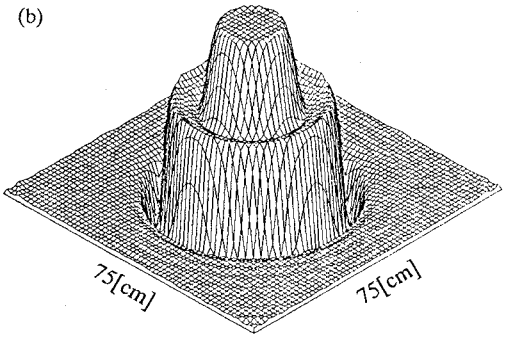

Fig. 3 The reconstructed image without the modification of projection function for radius 10cm and (a) ε_r = 1.1, (b) ε_r = 2.0.

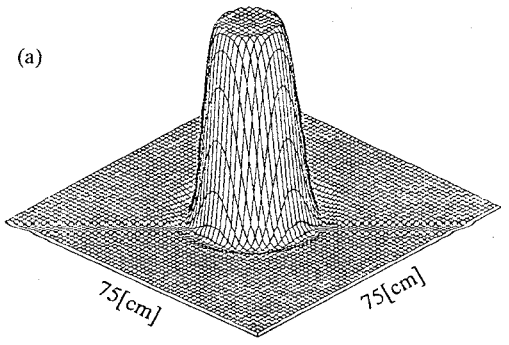

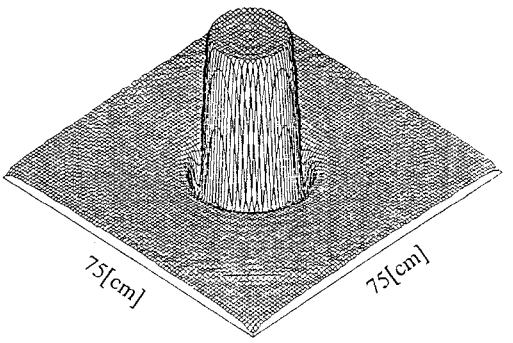

Fig. 4 The image improved by modifying the projection functions for Fig. 3(b).